# Transport properties in spherical quantum dots: Orbital-blockade and spin-blockade effects

C. F. Destefani and G. E. Marques
*Departamento de Física, Universidade Federal de São Carlos, Rodovia Washington Luiz, Km 235, 13565-905, São Carlos, São Paulo, Brazil*

C. Trallero-Giner
*Departamento de Física Teórica, Universidad de La Habana, 10400-La Habana, Cuba*
(Received 8 June 2001; revised manuscript received 17 December 2001; published 29 May 2002)

The conductance and the current of spherical quantum dots (SQD's) containing a small number of electrons are studied as a function of source-drain and gate voltages. The influences of magnetic field, spatial symmetry, electron-phonon interaction, dot radius, and temperature on the transport properties are analyzed. The many-particle states of the SQD's are described by the total spin ($S$) and total orbital ($L$) angular momenta ($LS$-coupling scheme) within the Hartree-Fock approximation, where the electron-electron interaction is included via a multipole expansion. The tunneling current is obtained by solving the master equation for the occupation number of the many-particle states of the system. The appearance of a negative differential conductance, due to the orbital-blockade mechanism directly related to the spherical central potential of the quantum dot, is reported.

DOI: 10.1103/PhysRevB.65.235314 PACS number(s): 73.23.Hk, 71.10.−w, 71.70.Ej

## I. INTRODUCTION

Many-body effects on the electronic properties of ultrasmall systems, such as charged quantum dots, have been studied in the last years due to their importance on the optical and transport properties. Several approaches, such as charging model,[1] correlated electron model,[2] Green's function,[3] and numerical methods (as Lanczos algorithm),[4] have been used in order to obtain the many-particle eigenstates and to study the transport properties in these novel systems. When the electronic density is small, a noncorrelated electron approach, such as the charging model, becomes a gross approximation and a microscopic treatment of the electron-electron interaction is required in order to reach a better understanding of the main processes taking place inside the system.[5] If the electron-electron interaction dominates over the thermal energy ($k_BT$), some mesoscopic characteristics of the transport of these systems such as Coulomb blockade, single electron tunneling oscillations and negative differential conductance (NDC) can be observed. The geometrical or spatial symmetry of the carriers localization region as well as the number of carriers in the system are extremely important ingredients to determine any quantum effect on the electronic structure which may be explored in device applications. Electron tunneling rates through a quantum dot are strongly influenced by the Coulomb interaction and the correlation present in few electron dot states leads to suppression of tunneling channels involving excited dot states.[6,7]

In this paper we will focus on the influence of the spherical geometry on the $I\times V$ characteristics of a system formed by a spherical quantum dot coupled to free electron leads by weak tunneling barriers. We will treat the system in the strongly confined and nonlinear regimes,[8] where both ground and excited states will play a role in the determination of the selection rules and the transition rates to and from the dot. Under a spherical symmetry profile plus an axial magnetic field both the spin and orbital angular momenta are good quantum numbers and the many-particle states, in the framework of the Hartree-Fock approximation, can be labeled according to the $LS$-coupling scheme. This type of coupling will impose spatial selection rules for the electronic transitions which, in turn, will govern the overall shape of the usual $I\times V$ curves. The effect of the total spin in a one-dimensional system have been already considered in the past (see Refs. 8,9). Nevertheless, a study of the spatial or geometrical symmetry and the confinement effects in the presence of an external magnetic field and their influence on the tunneling current should bring more details about the mechanisms which give origin to the NDC and to blockade effects. The magnetotunneling transport can provide a better understanding of the influence of the geometrical symmetry on a many-particle system, as Creffield *et al.*[11,12] and Akbar *et al.*[13] have recently studied for two-electron systems confined to different 2D-polygonal potential shapes. Also, magnetoexcitation spectra can be obtained from conductance measurements in the finite drain-source voltage region.[14,15]

The paper is organized as follows. In Sec. II we outline the theoretical model for the tunneling current in terms of the transition rates taking place on the transport processes through the dot. The Hartree-Fock model and the $LS$ scheme for a SQD including the effects of an external magnetic field on the many-particle states are also addressed. In Sec. III we study the general aspects of the profile in the $I\times V$ curves as a function of the temperature, magnetic field, and SQD parameters. Several features and differences of the blockade mechanisms associated to total spin and total orbital angular momenta are analyzed. Finally a summary of the obtained results is presented.

## II. TUNNELING CURRENT

In order to obtain the transport properties we will follow the same formalism described in Ref. 2 for one-dimensional systems. We consider a double barrier system formed by two

 

metallic leads linked to a SQD whose Hamiltonian can be separated as $H=H_0+H_P$. The unperturbed term $H_0=H_D+H_{ph}+H_R+H_L$, describes the isolated dot $H_D$, the phononic thermal bath $H_{\rm ph}$, and the left (right) free electron lead $H_L$ ($H_R$). In the second quantization formalism, each well known term in $H_0$ can be written as

$$H_{L(R)}=\sum_{\mathbf{k},\sigma}\varepsilon_{\mathbf{k}}^{L(R)}c^{+}_{L(R);\mathbf{k},\sigma}c_{L(R);\mathbf{k},\sigma},$$

$$H_{\rm ph}=\sum_{\mathbf{q}}\hbar\omega_{\mathbf{q}}\left(a_{\mathbf{q}}^{+}a_{\mathbf{q}}+\frac{1}{2}\right),$$

$$H_D=\sum_{\alpha,\sigma}(\varepsilon_\alpha-e\Phi)c^{+}_{\alpha,\sigma}c_{\alpha,\sigma}+\frac{1}{2}\sum_{\alpha_1,\alpha_2,\alpha_3,\alpha_4,\sigma_1,\sigma_2}\langle\alpha_1,\alpha_2|V_{ee}|\alpha_3,\alpha_4\rangle\times c^{+}_{\alpha_1,\sigma_1}c^{+}_{\alpha_2,\sigma_2}c_{\alpha_3,\sigma_2}c_{\alpha_4,\sigma_1}, \quad (1)$$

where $c^{+}_{L(R);\mathbf{k},\sigma}$ ($c_{L(R);\mathbf{k},\sigma}$), $a_{\mathbf{q}}^{+}$ ($a_{\mathbf{q}}$), and $c^{+}_{\alpha,\sigma}$ ($c_{\alpha,\sigma}$) are the creation (annihilation) operators for a free electron in the left (right) lead with energy $\varepsilon_{\mathbf{k}}^{L(R)}$ and wave vector $\mathbf{k}$, a phonon with energy $\hbar\omega_{\mathbf{q}}$ and wave vector $\mathbf{q}$ in the dot, and an electron in the quantum dot state $\alpha$ with confinement energy $\varepsilon_\alpha$, respectively. Also, $\sigma$ is the spin $z$ component, $-e\Phi$ is the external electrostatic potential applied to the system, and $\langle\alpha_1,\alpha_2|V_{ee}|\alpha_3,\alpha_4\rangle$ represents the electron-electron interaction energy inside the dot.

The perturbation Hamiltonian $H_P=H_L^T+H_R^T+H_{ep}$, takes into account the single electron transitions between the island and the left ($H_L^T$) and right ($H_R^T$) leads which are responsible for charging or discharging as well as the electron-phonon ($H_{ep}$) scattering processes occurring only inside the dot. The tunneling Hamiltonian $H_{L(R)}^T$ can be written in terms of the transition probability between the dot and the respective lead $T_{\mathbf{k},\alpha}^{L(R)}$ as

$$H_{L(R)}^T=\sum_{\mathbf{k},\alpha,\sigma}[T_{\mathbf{k},\alpha}^{L(R)}c^{+}_{L(R);\mathbf{k},\sigma}c_{\alpha,\sigma}+T_{\mathbf{k},\alpha}^{L(R)}{}^{*}c^{+}_{\alpha,\sigma}c_{L(R);\mathbf{k},\sigma}] \quad (2)$$

and the Fröhlich electron-phonon interaction is given by

$$H_{ep}=\sum_{\mathbf{q},\alpha_1,\alpha_2,\sigma}\sqrt{g(\mathbf{q},\alpha_1,\alpha_2)}c^{+}_{\alpha_1,\sigma}c_{\alpha_2,\sigma}(a_{\mathbf{q}}+a_{\mathbf{q}}^{+}), \quad (3)$$

with $\sqrt{g(\mathbf{q},\alpha_1,\alpha_2)}$ being the electron-phonon coupling constant.

The net dc current through the dot eigenstates can be calculated as[16,17]

$$I^{L(R)}=\mp e\sum_{i,j(j\neq i)}\overline{P_j}(\Gamma_{i,j}^{L(R)-}-\Gamma_{i,j}^{L(R)+}), \quad (4)$$

where $\Gamma_{i,j}^{L(R)}$ is the effective dot-to-left (right) lead transition rate and $\overline{P_i}$ is the stationary electron distribution function for the occupation of carriers in the state $i$. Equation (4) takes into account the balance between the number of electrons leaving ($-$) and entering ($+$) the dot per unit of time. The time evolution for the occupation probability $P_i$ of a given eigenstate is obtained as solution of the master equation

$$\frac{d}{dt}P_i=\sum_{j(j\neq i)}(\Gamma_{i,j}P_j-\Gamma_{j,i}P_i), \quad (5)$$

under normalization condition $\Sigma_i P_i=1$, and $\Gamma_{i,j}$ being the total effective transition rate (dot-leads plus electron-phonon scattering) between states of the dot. In the case of stationary occupation of the states ($dP_i/dt=0$) one can easily solve Eq. (5) and obtain the stationary distribution function $\overline{P_i}$ for the $i$th state.

### A. Transition rates

Assuming a weak coupling limit described by the interaction Hamiltonian $H_P$, the transition probability per unit of time of a carrier to jump in or out the system can be calculated by using Fermi's golden rule

$$\gamma_{j,i}=\left(\frac{2\pi}{\hbar}\right)|\langle\Psi_j^{(0)}|H_P|\Psi_i^{(0)}\rangle|^2\delta(E_j^{(0)}-E_i^{(0)}), \quad (6)$$

where $E_i^{(0)}$ ($E_j^{(0)}$) and $\Psi_i^{(0)}$ ($\Psi_j^{(0)}$) are the energy and wave function at the initial (final) state of the unperturbed system. Each state of the Hamiltonian $H_0$ can be written in the form $|\Psi^{(0)}\rangle=|\Psi_D\rangle\otimes|\Psi_L\rangle\otimes|\Psi_R\rangle\otimes|\Psi_{\rm ph}\rangle$ with eigenvalue $E^{(0)}=E_D+\varepsilon_{\mathbf{k}}^{L}+\varepsilon_{\mathbf{k}}^{R}+\hbar\omega_{\mathbf{q}}$ and $E_D$ being the $N$-particle eigenenergy solution of $H_D$.

The effective transition rates between states $D_j$ and $D_i$ of the SQD are given by

$$\Gamma_{D_j,D_i}=\left\langle\sum_{L_j,R_j,\mathbf{q}_j}\gamma_{j,i}\right\rangle_{th(L_i,R_i,\mathbf{q}_i)}, \quad (7)$$

where the sum runs over all final states of the free electrons in the leads that are coupled to the thermal reservoir and to the phonon field. Also, each matrix element in $\gamma_{j,i}$ is calculated under initial thermal equilibrium condition. For simplicity, we will neglect any dependence of all coupling parameters on quantum numbers by setting $T_{\mathbf{k},\alpha}^{L(R)}\equiv T^{L(R)}$ and $\sqrt{g(\mathbf{q},\alpha_1,\alpha_2)}\equiv\sqrt{g}$. Moreover, in the sum over leads and phonon states, we will relabel the dot states $|\Psi_{D_i}\rangle$ as $|\Psi_I\rangle$. Thus, all allowed transitions which enter in Eq. (4) can be written as

$$\Gamma_{I,J}^{L(R)-}=\frac{1}{2}t^{L(R)}[1-f_{L(R)}(E)]B_{I,J}\delta_{n_I,n_J-1}, \quad (8)$$

$$\Gamma_{J,I}^{L(R)+}=\frac{1}{2}t^{L(R)}[f_{L(R)}(E)]C_{J,I}\delta_{n_J,n_I+1}, \quad (9)$$

$$\Gamma_{J,I}^{ph-}=r[n_B(\hbar\omega_{\mathbf{q}})]D_{J,I}\delta_{n_J,n_I}, \quad (10)$$

$$\Gamma_{I,J}^{ph+}=r[1+n_B(\hbar\omega_{\mathbf{q}})]D_{I,J}\delta_{n_I,n_J}. \quad (11)$$

The first two terms are the tunneling rates controlling the decrease or increase of the occupation number in the SQD by one electron. The third and fourth terms take into account the electron scattering rates due to the absorption or emission of one phonon in the SQD. In Eqs. (8)–(11) $f_{L(R)}(E)$ and $n_B(\hbar\omega_{\mathbf{q}})$ are the Fermi-Dirac and Bose-Einstein distribution functions and $f_{L(R)}(E)$ is calculated at $E=E_J^{(0)}-E_I^{(0)}$ including the chemical potential $\mu^{L(R)}$ of the respective lead. Also, $t^{L(R)}$ and $r$ are the renormalized transmission and the inelastic scattering rates, respectively, given by

$$t^{L(R)}=\frac{2\pi}{\hbar}|T^{L/R}|^2\rho_{L(R)}(E), \qquad r=\frac{2\pi}{\hbar}g\rho(ph)(\hbar\omega_{\mathbf{q}}), \tag{12}$$

where $\rho_{L(R)}(E)$ $[\rho_{\mathrm{ph}}(\hbar\omega_{\mathbf{q}})]$ is the electron (phonon) density of states in the leads (dot). Finally,

$$B_{I,J}=|\sum_{\alpha,\sigma}\langle\Psi_I|c_{\alpha,\sigma}|\Psi_J\rangle|^2, \tag{13}$$

$$C_{J,I}=|\sum_{\alpha,\sigma}\langle\Psi_J|c^+_{\alpha,\sigma}|\Psi_I\rangle|^2, \tag{14}$$

$$D_{J,I}=|\sum_{\alpha_1,\alpha_2,\sigma}\langle\Psi_J|c^+_{\alpha_1,\sigma}c_{\alpha_2,\sigma}|\Psi_I\rangle|^2, \tag{15}$$

are the matrix elements between SQD many-particle states which determine the selection rules for the involved processes. The total effective transition rate which enters in Eq. (5) is given by $\Gamma=\Gamma^{L+}+\Gamma^{R+}+\Gamma^{L-}+\Gamma^{R-}+\Gamma^{\mathrm{ph}+}+\Gamma^{\mathrm{ph}-}$.

### B. Hartree-Fock spectrum of a spherical quantum dot in a magnetic field

The goal of the present paper is to evaluate the transition rates and transport properties through the many-particle states in a SQD under an external magnetic field. The confining potential of the dot is modeled by an infinite spherical barrier of radius $R_0$. The normalized single-particle wave functions can be written as

$$|\alpha;\sigma\rangle=|n,l,m_l\rangle\otimes|s,m_s\rangle=\left[\frac{2}{R_0^3}\frac{1}{[j_{l+1}(\alpha_{nl})]^2}\right]^{1/2}\times|j_l(\alpha_{nl}x)\rangle|Y_{l,m_l}(\theta,\phi)\rangle\otimes|s,m_s\rangle, \tag{16}$$

where $x=(r/R_0)$, $j_l(\alpha_{nl}x)$ is the spherical Bessel function of order $l$ for the $n$th level, $\alpha_{nl}$ its zero, $Y_{l,m_l}(\theta,\phi)$ is the spherical harmonic, and $|s,m_s\rangle$ is the spin eigenfunction with $s=1/2$ and $m_s=\pm 1/2$.

In order to obtain the $N$-particle eigenstates we have chosen to work within the $LS$-coupling scheme and label the states according to the total orbital $\mathbf{L}=\Sigma\mathbf{l}_i$ and total spin $\mathbf{S}=\Sigma\mathbf{s}_i$ angular momenta. Each state will be a linear combination of Slater determinants of the single-particle states $|n,l,m_l\rangle\otimes|s,m_s\rangle$ times the corresponding Clebsch-Gordan coefficients $C^{j_1,j_2,j_3}_{m_1,m_2,m_3}=\langle j_1,m_1;j_2,m_2|j_3,m_3\rangle$ for the angular momenta coupling. Hence, we need to construct all possible antisymmetric Hartree-Fock eigenstates for a dot with a given occupation number $N$. For the simplest case $N=2$ we have

$$|LM_L,SM_S\rangle=\sum_{l_1,l_2,m_{l_1},m_{l_2}}C^{l_1,l_2,L}_{m_{l_1},m_{l_2},M_L}|l_1,m_{l_1}\rangle|l_2,m_{l_2}\rangle\times\sum_{s_1,s_2,m_{s_1},m_{s_2}}C^{s_1,s_2,S}_{m_{s_1},m_{s_2},M_S}\||s_1,m_{s_1}\rangle|s_2,m_{s_2}\rangle\| \tag{17}$$

or

$$|LM_L,SM_S\rangle=\sum_{l_1,l_2,m_{l_1},m_{l_2}}C^{l_1,l_2,L}_{m_{l_1},m_{l_2},M_L}\||l_1,m_{l_1}\rangle|l_2,m_{l_2}\rangle\|\times\sum_{s_1,s_2,m_{s_1},m_{s_2}}C^{s_1,s_2,S}_{m_{s_1},m_{s_2},M_S}|s_1,m_{s_1}\rangle|s_2,m_{s_2}\rangle, \tag{18}$$

where $\||j_1,m_1\rangle|j_2,m_2\rangle\|$ is a Slater determinant under the conditions $|l_1-l_2|<L<|l_1+l_2|$ and $|s_1-s_2|<S<|s_1+s_2|$. Within the usual spectroscopic notation $^{2S+1}L$, the ground state is $^1S$ and the first excited levels are the $^3P$ states (triplet) described by Eq. (18) and $^1P$ states (singlet) given by Eq. (17). In the same way, the case $N=3$ can be obtained by the combination of three-particle states (see Ref. 18) with the restricting conditions $|l_1-l_2|<L'<|l_1+l_2|$, $|L'-l_3|<L<|L'+l_3|$, $|s_1-s_2|<S'<|s_1+s_2|$, and $|S'-s_3|<S<|S'+s_3|$. In all expressions the index $n_i$ was omitted since we are dealing with the lowest excited states and small occupation number. Thus the above linear combinations involve only $n_i=1$ radial functions.

The Coulomb interaction $V_{ee}(\mathbf{r}_1,\mathbf{r}_2)=e^2/(\varepsilon|\mathbf{r}_1-\mathbf{r}_2|)$, is treated in the usual multipole expansion

$$V_{ee}(\mathbf{r}_1,\mathbf{r}_2)=\frac{e^2}{\varepsilon}\sum_{\kappa=0}^{\infty}\frac{4\pi}{2\kappa+1}\frac{r_<^\kappa}{r_>^{\kappa+1}}\sum_{m_\kappa=-\kappa}^{\kappa}(-1)^{m_\kappa}\times Y_{\kappa,-m_\kappa}(\theta_1,\phi_1)Y_{\kappa,m_\kappa}(\theta_2,\phi_2), \tag{19}$$

where $\mathbf{r}_1$ and $\mathbf{r}_2$ are the electron coordinates, $\varepsilon$ is the dielectric constant of the dot, and $r_<$ ($r_>$) is the smaller (larger) value between the radial coordinates $r_1$ and $r_2$. Let us define the different energy contributions $F^\kappa$ and $G^\kappa$ in terms of direct $\Gamma^\kappa$ and exchange $\Lambda^\kappa$ radial integrals of the electron-electron interaction as

$$F^\kappa(n_1l_1,n_2l_2)=\frac{e^2}{\varepsilon R_0}\Gamma^\kappa(n_1l_1,n_2l_2), \tag{20}$$

$$G^\kappa(n_1l_1,n_2l_2)=\frac{e^2}{\varepsilon R_0}\Lambda^\kappa(n_1l_1,n_2l_2). \tag{21}$$

Coulomb energies for the cases with $N=2$ and $N=3$ particles in terms of $F^\kappa$ and $G^\kappa$ and the corresponding numerical values of the integrals $\Gamma^\kappa$ and $\Lambda^\kappa$ are given in the Appendix.

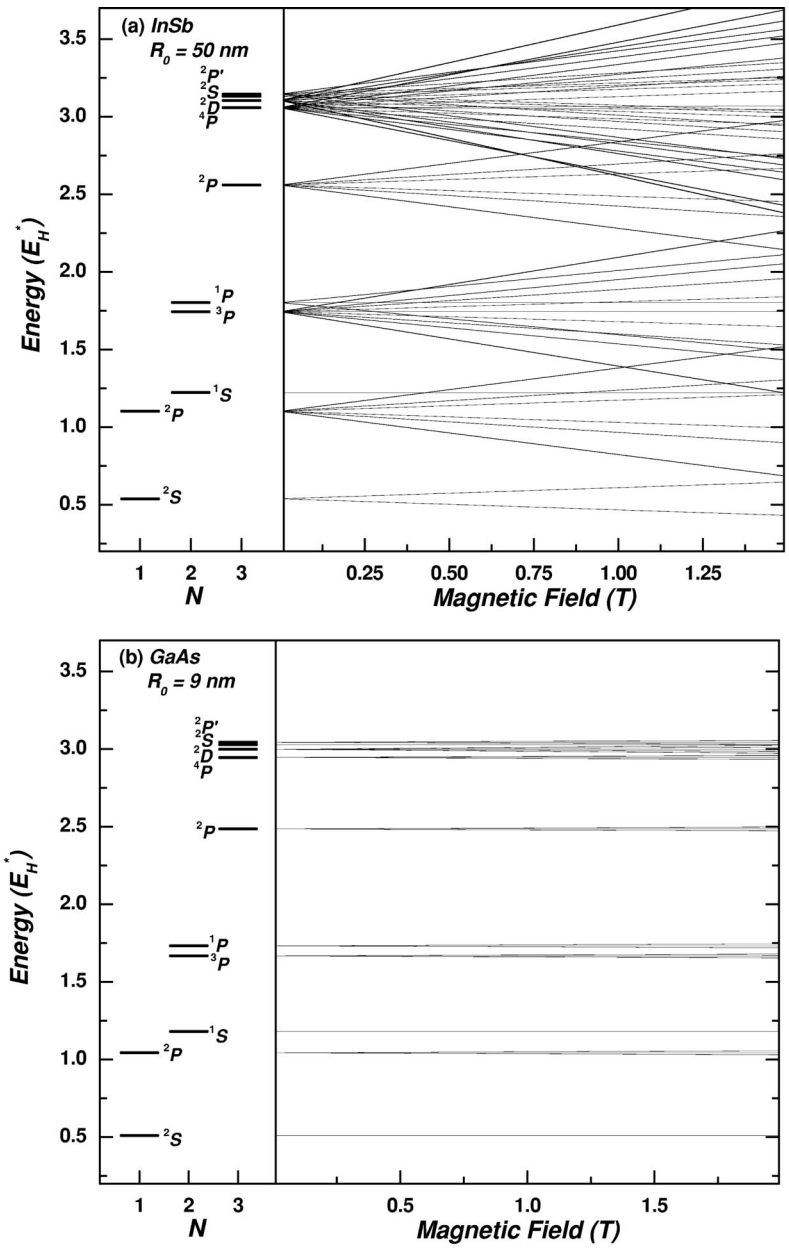


FIG. 1. Energy levels for $N=1$, 2, and 3 particles, in spherical quantum dots under an applied magnetic field, measured in units of effective Hartree energy. The levels are indicated by the spectroscopic notation $^{2S+1}L$, according to the $LS$ scheme. (a) InSb dot with radius $R_0=50$ nm; (b) GaAs dot with $R_0=9$ nm. The Zeeman and spin splittings lift the degeneracy of the many-particle states and the strong Landè $g$ factor for InSb causes level crossings leading to changes in the level sequence above special values of the magnetic field.

In the presence of an external magnetic field $\mathbf{B}=(0,0,B_0)$ and neglecting the term proportional to $B_0^2$ we just add to the SQD many-particle energies the term

$$E_B=\mu_B^* B_0\left(M_L+M_S\frac{gm^*}{m_0}\right), \tag{22}$$

where $\mu_B^*=e\hbar/(2m^*c)$ is the effective Bohr magneton, $m^*$ ($m_0$) is the effective (free) electron mass, and $g$ is the effective Landè factor of the SQD. Such approximation is valid when the Zeeman $\mu_B^* B_0 M_L$ ($B_Z$) and spin $\mu_B^* B_0 M_S g m^*/m_0$ ($B_S$) splittings are stronger than $e^2B_0^2\langle r^2\rangle/(8m^*c^2)$. By taking $\langle r^2\rangle$ in the ground state the conditions to be fulfilled are

$$B_0<B_Z=\frac{14.3M_L}{R_0^2}\frac{\hbar c}{e},\qquad B_0<B_S=\frac{14.3M_S}{R_0^2}\frac{\hbar c}{e}\frac{gm^*}{m_0}. \tag{23}$$

For the sake of comparison and further discussion, in Fig. 1 we are showing the quasiparticle energy levels as a function of the magnetic field for InSb [Fig. 1(a)] and GaAs [Fig. 1(b)] SQD's with radius $R_0=50$ nm and $R_0=9$ nm, respectively. We have considered dots charged with one, two, and three carriers at $\Phi=0$. For the calculations the values of $m^*_{\mathrm{InSb}}=0.013\ m_0$, $g_{\mathrm{InSb}}=-53.1$, $\varepsilon_{\mathrm{InSb}}=16.5$, $m^*_{\mathrm{GaAs}}=0.065\ m_0$, $g_{\mathrm{GaAs}}=0.45$, and $\varepsilon_{\mathrm{GaAs}}=12.65$ have been used. At $B_0=0$ the ground states have total spin $S=0$ ($N=2$) and $S=1/2$ ($N=1,3$), while the lowest excited states, $^3P$ for $N=2$ and $^4P$ for $N=3$, are spin polarized states with maximum values $S=1$ and $S=3/2$, respectively. The effective Bohr radius $a_B^*=\varepsilon\hbar^2/(m^*e^2)$ and the effective Hartree energy $E_H^*=e^2/a_B^*$, for InSb and GaAs are $a^*_{B(\mathrm{InSb})}=67.1$ nm, $a^*_{B(\mathrm{GaAs})}=10.3$ nm, $E^*_{H(\mathrm{InSb})}=21.4$ meV, and $E^*_{H(\mathrm{GaAs})}=140$ meV. In the case $R_0<a_B^*$ the carriers are in the strong confined regime and the electron-electron interac-

tion becomes a perturbation to the total energy of the system. Due to the dependence of $E_B$ on the magnetic field, the degeneracy on the quantum numbers $M_L$ and $M_S$ is lifted at $B_0 \neq 0$. Since the modulus of the effective Landè $g$ factor in InSb is two orders of magnitude larger than in GaAs, one may observe for InSb SQD in Fig. 1(a) a set of quasiparticle level crossings. These crossings are completely absent for GaAs SQD even for high magnetic fields [Fig. 1(b)]. The electron-electron interaction in the spherical region determines the sequence of energy states but the magnetic energy $E_B$ can change this sequence, as can be observed for the $^2P$, $^4P$, and $^2D$ states in InSb with $N=3$ at $B_0 > 0.71$ T. These level crossing effects, which depend on the field, dot radius, and effective $g$ factor, should have influence on the magnetotransport properties of charged dots as will be shown in Sec. III. It should also be mentioned that different spatial symmetries can produce different ordering of excited states, as can be observed in Refs. 2,5, where a square dot geometry was considered and the spin polarized states at $B_0=0$ had higher energy than the unpolarized ones.

According to the Hartree-Fock model and in the framework of the $LS$-coupling scheme the matrix elements in Eqs. (13)–(15) involved in the transport processes are given by

$$C_{J,I} = \Big|\sum_{l,m_l} \langle L_J M_{L_J} | c^+_{l,m_l} | L_I M_{L_I} \rangle\Big|^2 \times \Big|\sum_{s,m_s} \langle S_J M_{S_J} | c^+_{s,m_s} | S_I M_{S_I} \rangle\Big|^2, \tag{24}$$

with an analogous equation for $B_{I,J}$. Here, the initial state $(L_I, S_I)$ of the dot is coupled to the final state $(L_J, S_J)$ through the momenta $(l,s)$ of the transition electron. The Clebsch-Gordan coefficients induce the selection rules

$$\left\{ \begin{array}{ll} S_J = S_I \pm 1/2, & M_{S_J} = M_{S_I} \pm 1/2, \\ L_J = L_I, L_I \pm 1, & M_{L_J} = M_{L_I}, M_{L_I} \pm 1 \end{array} \right\}. \tag{25}$$

Finally, and due to phonons, the electronic transitions should occur only between states with the same quantum numbers.[19] Hence, the matrix elements $D_{J,I}$ must satisfy

$$D_{J,I} = \delta_{L_J,L_I} \delta_{M_{L_J},M_{L_I}} \delta_{S_J,S_I} \delta_{M_{S_J},M_{S_I}}. \tag{26}$$

## III. TRANSPORT PROPERTIES AND ORBITAL BLOCKADE

We have calculated the current in the system modeled above as a function of both source-drain voltage, $V_{sd} = (\mu^L - \mu^R)/e$ (current curves), and applied gate voltage $\Phi$ (conductance curves). Let us first discuss the general aspects of these $I \times V$ curves for $\Phi = 0$, as summarized in Figs. 2(a) and 2(b) for an InSb SQD with radius $R_0 = 15$ nm and $R_0 = 50$ nm, respectively.

The simplest point is the effect of temperature on the system. At low temperatures the curves show structures due to the Coulomb interaction between carriers, that appear as steps in the current and as peaks in the conductance curves, when the dot is being charged with $N=1$, 2, and 3 electrons. As the temperature is increased, the steps become smoother while the height (width) of peaks decreases (increases) accordingly.

The position of each step in the current curve is related to a resonant transition between two dot states whereas the length of each plateau should equal the difference between two consecutive resonances. The height of each step is associated to the net charge of the states involved in the transition. Another important aspect in the current is the occurrence of NDC regions at some special voltages, that will be discussed later. The peaks in the conductance occur at voltages where the involved ground state for $N=1$, 2, 3 reaches its maximum net charge. Notice also a ratio 2 between peak heights for $N=3$ if compared with the first two conductance peaks ($N=1$, 2), a difference directly related to the many-body effects as well as to the spatial symmetry of the confining region that are present in all many-particle ground states. In the charging model, where electron-electron interaction is assumed as a constant, the height and separation of all peaks in the conductance, as well as the height and length of all plateaus in the current, are more regular.

The importance of the spatial symmetry will be addressed later, although, the expected influence of the size of the confining region in the $I \times V$ curves can be seen in Fig. 2(b). As the dot radius increases, the energy separation between excited states is reduced and the plateaus in the current, as well as the separation between peaks in the conductance, become shorter. However, the other qualitative features are equal to the case shown in Fig. 2(a). The same behavior is observed in GaAs SQD's with different radii.

The current curves calculated at $B_0=0$ and temperature $(k_B T = 0.003 E_H^*)$ smaller than the energy level separation of an InSb SQD with $R_0 = 50$ nm are shown in Fig. 3. For each curve the Hatree-Fock states were calculated with the value of gate voltage running from 0 (bottom) to 0.2 $E_H^*/e$ (top). Clearly, a constant $\Phi$ only causes a rigid shift $e\Phi$ in each Hartree-Fock energy to a lower value. Yet, the ordering of states and the sequence of transitions between them are not affected with increasing gate voltages. The main feature occurring at different values of $\Phi$ is the suppression of the third plateau of the Coulomb blockade above $\Phi = 0.13\ E_H^*/e$ (shown as dotted line). In the inset of Fig. 3, we show the overall shape of the $I \times V$ curves for different configurations of the dot many-particle states and their symmetries in the following situations: (i) $LS$-coupling scheme, (ii) $S$ contribution disregarding the orbital angular momentum selection rules, and (iii) $L$ contribution not including the spin selection rules. It can be seen that the $\Delta L = 0, \pm 1$ selection rules reduce the total current as compared to the spin contribution case. This effect is due to the fact that $L$, having only integer quantum numbers, and $S$, having alternated sequence of integer and half-integer quantum numbers, produce different step heights in the blockade and NDC regions. The $LS$-coupling scheme will mix the spatial symmetry and spin effects at different values of $V_{sd}$, giving origin to wider and smoother blockade and NDC regions. This inset also shows (dotted lines) the changes in the current as induced by a finite gate voltage in the same three configurations listed above.

In order to help our discussion of the aspects induced by

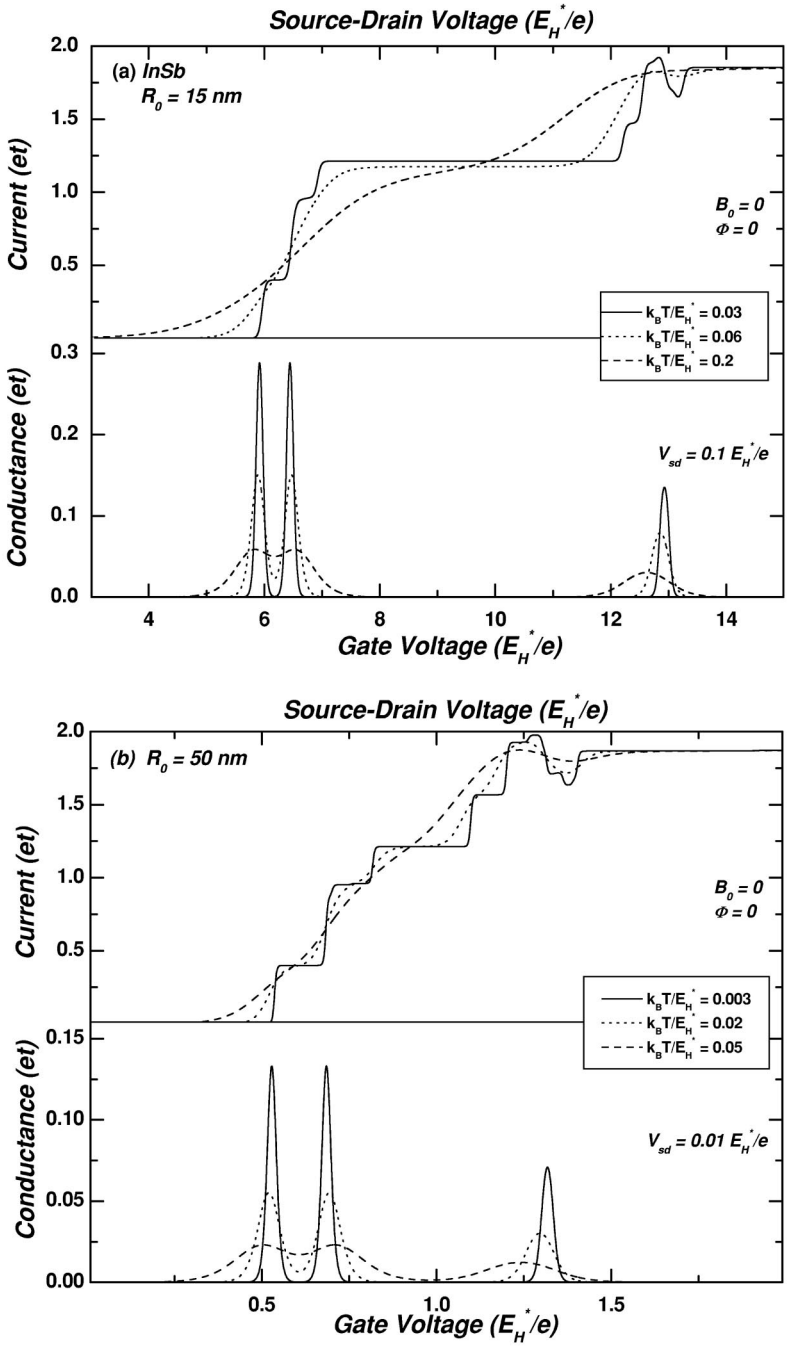


FIG. 2. General aspects of $I\times V$ characteristics in InSb SQD's at different temperatures and zero magnetic field. Current as function of source-drain voltage $V_{sd}$ (top) and conductance as function of gate voltage $\Phi$ (bottom). (a) Dot with radius $R_0=15$ nm; (b) dot with $R_0=50$ nm. The current is measured in units of $et$, where the transmissivity is $t=t^Lt^R/(t^L+t^R)$, while both voltages are measured in units of $E_H^*/e$.

the change in the gate voltage, in Fig. 4 we are presenting the first [Fig. 4(a), $\Phi=0$] and the last [Fig. 4(b), $\Phi=0.2E_H^*/e$] curves of Fig. 3 together with the respective population analysis of each dot state, as a function of the source-drain voltage. The details leading to the origin of each step and the NDC regions in Fig. 4(a) are as follows. From $V_{sd}=0$ to $V_{sd}=0.54\ E_H^*/e$ the current is zero since the SQD is not yet populated. At this value of the source-drain voltage occurs the first transition to the ground state $^2S_1$ for $N=1$. Notice, from now on, an added subscript in the labeling of states in order to distinguish the number of particles in the dot. The second step at 0.68 appears when the transition $^2S_1\rightarrow{}^1S_2$ occurs and the ground state for $N=2$ begins to be populated. Also, the charge of states $^2P_1$, $^3P_2$ are being built (off-resonance) even though the allowed resonant transitions to these states only occur at higher values of $V_{sd}$. Just at the edge of this second step, at 0.70, the transition $^2P_1\rightarrow{}^1P_2$ is activated and produces a very small blockade. Another detail that should be pointed is that the transitions $^2P_1\rightarrow{}^1S_2$ and $^2P_1\rightarrow{}^3P_2$ should have occurred before, at 0.12 and 0.64, respectively, however, the steps in the current are not observed since the initial state was not populated yet. In the center of the second plateau, at 0.75, the transition $^1P_2\rightarrow{}^2P_3$ is then activated and the ground state for $N=3$ begins to receive charge.

The third step in the current, at $V_{sd}=0.81\ E_H^*/e$, leads to the next plateau due to the resonant transition $^3P_2\rightarrow{}^2P_3$. The third plateau ends up only when the source-drain voltage

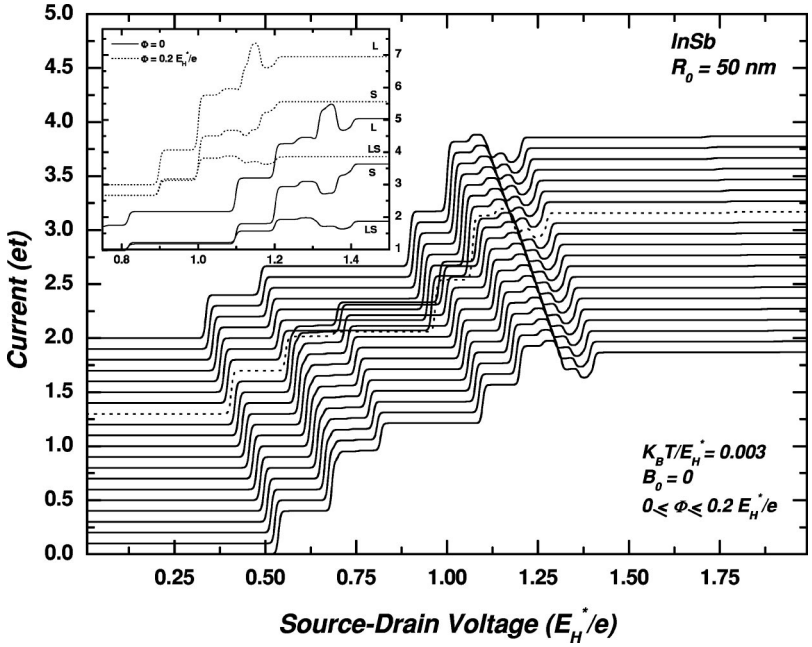


FIG. 3. Influences of a finite gate voltage $\Phi$ in the current curves for an InSb dot with $R_0 = 50$ nm, at zero magnetic field. The plots shown are in steps of $0.01E_H^*/e$, ranging from $\Phi = 0$ to $0.2\ E_H^*/e$. The current at $\Phi = 0.13\ E_H^*/e$, where the suppression of the third plateau has occurred, is shown in dotted line. The inset compares, at two gate voltages, the influences on the current in different configurations of the Hartree-Fock states in a SQD: *L* curve (no *S*-selection rules), *S* curve (no *L*-selection rules), and *LS* curve with both selection rules.

reaches the value 1.10. At this value, the allowed resonant transition to the state $^2P_1$ produces the fourth step in the current curve. Here again many states show exchange in their population: $^2S_1$, $^1S_2$ are being depopulated while $^3P_2$, $^1P_2$, $^2P_3$, $^2P_1$ are being populated, but the allowed resonant transitions between them only occur at different values of $V_{sd}$. The fifth step at 1.20 is mainly due to the transition $^2S_1 \rightarrow {}^3P_2$, although the states $^1S_2$ ($^2P_1$, $^1P_2$, $^2P_3$) are losing (gaining) fractions of the total population at this voltage. When we reach the value 1.25, the transition $^1P_2 \rightarrow {}^4P_3$ should be observed, however, this does violate the *S*-selection rules and the step is not seen in the curve. Moreover, just at 1.26, the allowed resonant transition $^2S_1 \rightarrow {}^1P_2$ is activated and, only then, we can see the sixth step in the current.

In the sequence we reach the NDC regions where there are eight possible resonant energies in the interval 1.3–1.4. Here, only states with $N=3$ are increasing their populations while the other states with $N=1, 2$ are being depopulated. When the voltage reaches the values 1.30 and 1.31, which are, respectively, the resonant energies for the transitions $^1P_2 \rightarrow {}^2D_3$ and $^3P_2 \rightarrow {}^4P_3$, the current does not increase but, instead, shows its first decrease or NDC region. Although these transitions are allowed, we see that the spin polarized $^4P_3$ state becomes the most populated in this interval, at the expenses of a discharge of other dot states, mainly $^2P_1$, $^3P_2$, $^1P_2$, and $^2P_3$. Thus, due to spin selection rules, the lifetime of this spin polarized state becomes very high, and the probability for the system to leave this state to another unpolarized configuration decreases drastically. We can therefore identify this first decrease in the current as caused by a spin-blockade phenomenon.[9,10] Right after, at voltages 1.32, 1.33, and 1.34, the transitions $^1P_2 \rightarrow {}^2S_3$, $^1S_2 \rightarrow {}^2P_3$, and $^1P_2 \rightarrow {}^2P_3'$ are, respectively, activated. Here, the spin polarized state loses a fraction of its population and the current stays in the short plateau, just before the next NDC region.

At voltages 1.36 and 1.38, the resonances for transitions $^3P_2 \rightarrow {}^2D_3$ and $^3P_2 \rightarrow {}^2S_3$, we define the interval of the second NDC region. We see that the $^2D_3$ state gains almost all of its population at 1.36 (the beginning of the region), accompanied by a decrease in the spin polarized $^4P_3$ state. Observe that this is the state with the highest orbital angular momentum ($L=2$) and, according to the *L*-selection rules, its effective lifetime becomes very large. The system becomes trapped in this state, as occurred for the $^4P_3$ state, with a small probability to leave it. Therefore, we can identify this second NDC region as caused by an *L* blockade, which we have named the ''orbital blockade.'' Such a blockade mechanism is totally caused by the spatial properties and the symmetry profile of the system, and certainly would not be present in the current had we considered only the spin degree of freedom for the system.

At $V_{sd} = 1.38E_H^*/e$ (the end of the region), both $^2D_3$ and $^4P_3$ states have lost fractions of their populations and, at 1.40, the transition $^3P_2 \rightarrow {}^2P_3'$ is activated, leading to an increase in the current and only then the system leaves the second NDC region to reach the last plateau. Here we would notice that the current has a smaller value than the one just before the first NDC region. The reason for the difference is that the two worst conducting states, the spin polarized $^4P_3$ and the highest orbital angular momentum $^2D_3$ states, are the most populated ones at high voltages. There is another extremely small blockade in the interval 1.83–1.92, due to the activation of the set of transitions $^1S_2 \rightarrow \{{}^4P_3, {}^2D_3, {}^2S_3, {}^2P_3'\}$. The first two are blockaded, respectively, by *S* and *L* selection rules, and the last two almost do not contribute to the current because of the respective small population reached by these states.

Let us now discuss the origin of the suppression of the third step in the current, occurring above a given value of gate voltage $\Phi = 0.13E_H^*/e$ (see Fig. 3). A comparison between the population of the states in the cases shown in Figs.

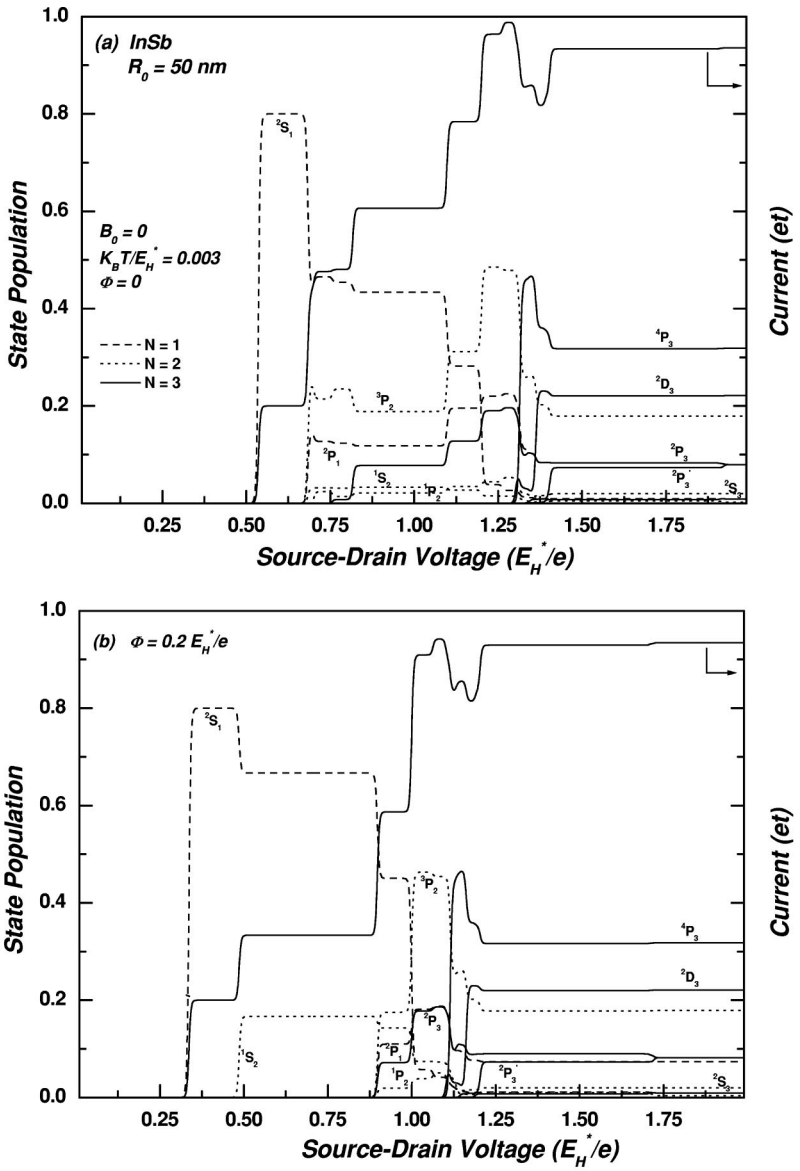


FIG. 4. Population (charge formation) analysis for the first [(a) with $\Phi=0$)] and the last [(b) with $\Phi=0.2\ E_H^*/e$] curves of Fig. 3 showing those states taking place in the current and in the NDC regions. Dashed lines show charge formation in the two lower states of the SQD for $N=1$. Dotted lines are the occupation for the first three states for $N=2$. Solid lines represent the charge formation for the first five levels for $N=3$. The sequence of states for $N=1$, 2, and 3 particles is shown in Fig. 1(a).

4(a) and 4(b) is needed in order to understand these effects. The new and predominant aspects of the $I\times V$ curves without magnetic field as $\Phi$ increases are: (i) the decrease in the length of the zero plateau, when the SQD is fully empty, (ii) the suppression of the third plateau in the current, and (iii) the best definition of the two valleys in the NDC region.

It is clear that the absence of the third step, at high values of gate voltages, was caused by the suppression of the transition $^3P_2\rightarrow{}^2P_3$, which produces most of the height of this step at low voltages. Moreover, the two much less important transitions in the second plateau, $^2P_1\rightarrow{}^1P_2$ (at edge) and $^1P_2\rightarrow{}^2P_3$ (at the center), are also suppressed. It becomes clear in Fig. 4(b) that these suppressions have occurred because the respective initial states, which are populated for small values of $\Phi$, will be empty above a given value of the gate voltage. Strictly, the states $^2P_3$, $^1P_2$, $^3P_2$, and $^2P_1$, directly involved in these suppressions, will contribute to the current only close to the NDC region. Also, the relative height of the steps, at finite $\Phi$, will change accordingly to the amount of charge built into the states. Furthermore, in Fig. 4(b), we can observe the occurrence of two well defined valleys characterizing the two distinct NDC regions with the current in the last plateau reaching a value practically equal to the one just before the NDC regions, in contrast with the case $\Phi=0$ where it is smaller. All these new features were caused by the induced redistribution in the population of the states in presence of finite gate voltages.

As a final observation, the inset of Fig. 3 shows that the $L$ blockade always dominates over the $S$ blockade. Notice that the NDC region in the $L$ curve is much less affected by the change in the gate voltage than in the $S$ curve. The spherical symmetry restrain present in the many-particle states plays an important role on the transport properties, in special, close to the NDC regions. The effectiveness of the orbital blockade seems stronger than the spin-blockade in the transport of SQD's. It is clear from Figs. 4(a) and 4(b), that the discharge (lifetime) of the $^4P_3$ state is larger (smaller) than the $^2D_3$ state across the NDC regions, a property directly linked to the differences in the selections rules for the orbital and spin angular momenta. It is important to remark that the above

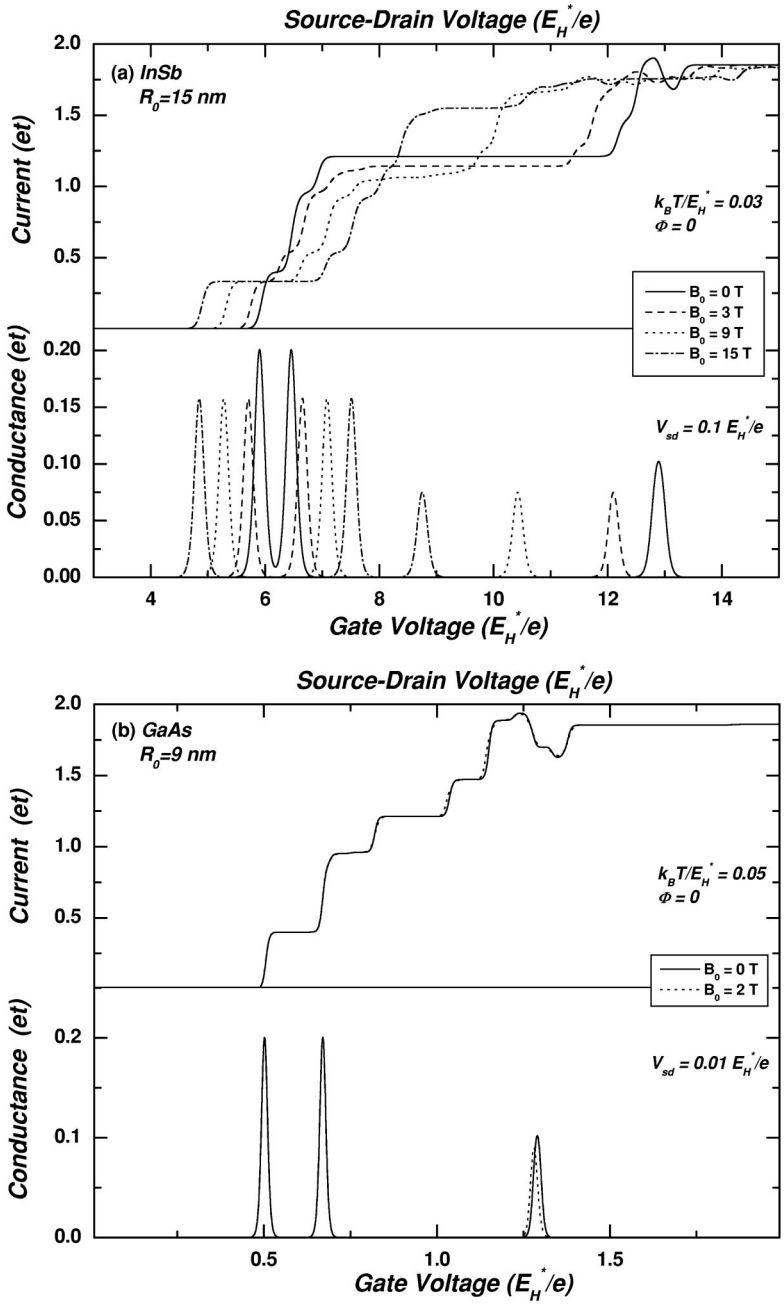


FIG. 5. Influences of a magnetic field on the $I\times V$ characteristics of SQD's at a constant temperature. (a) Current and conductance curves in InSb dot with $R_0=15$ nm. (b) Current and conductance curves in GaAs dot with $R_0=9$ nm. The external magnetic field has negligible influence on the transport properties on GaAs due to its smaller range of validity, if one considers only the linear dependence on the field. For larger values of the magnetic field, the diamagnetic term must be included. The units and notation are the same as in Fig. 2.

conclusions are strictly valid under the condition $R_0<a_B^*$, where the eigenfunctions in Eq. (16) are a good set of single-particle wave functions in the SQD and, thus, the electron-electron interaction can be considered as a perturbation to the system.

The general aspects of the influence of a magnetic field on the $I\times V$ curves are analyzed in Fig. 5(a) for InSb and in Fig. 5(b) for GaAs. Due to the larger value of the effective Landè $g$ factor of InSb SQD and the smaller radius in comparison with $a_B^*$ ($R_0=15$ nm), the applied magnetic field can be varied in the interval $0<15$ T. For GaAs SQD ($R_0=9$ nm) $B_0$ is restricted to values smaller than 2 T [see Eq. (23)]. The effects of an increase in the magnetic field in InSb dots are as follows. (i) New small NDC regions appear in the current, below and above those two existing at zero field, an effect directly linked to the magnetic energy of levels, their dependence on the quantum numbers $M_L$ and $M_S$ [see Fig. 1(a)] and their respective selection rules. (ii) A decrease in the sizes and depths of the NDC regions due to an increase in the number of possible transitions which can change the maximum charge (discharge) in each state responsible for the blockade mechanisms. (iii) For materials with a large $g$ factor the ordering of excited levels, which are responsible for the NDC regions, can be exchanged at specific values of $B_0$.

A clear signature of the induced change in the sequence of the levels, as caused by the Zeeman and spin splittings, is more apparent in the conductance peak positions in Fig. 5(a), where the peak separation between $N=1$ and $N=2$ ($N=2$ and $N=3$) increases (decreases) as a function of the magnetic field. The peaks in the conductance curves also show

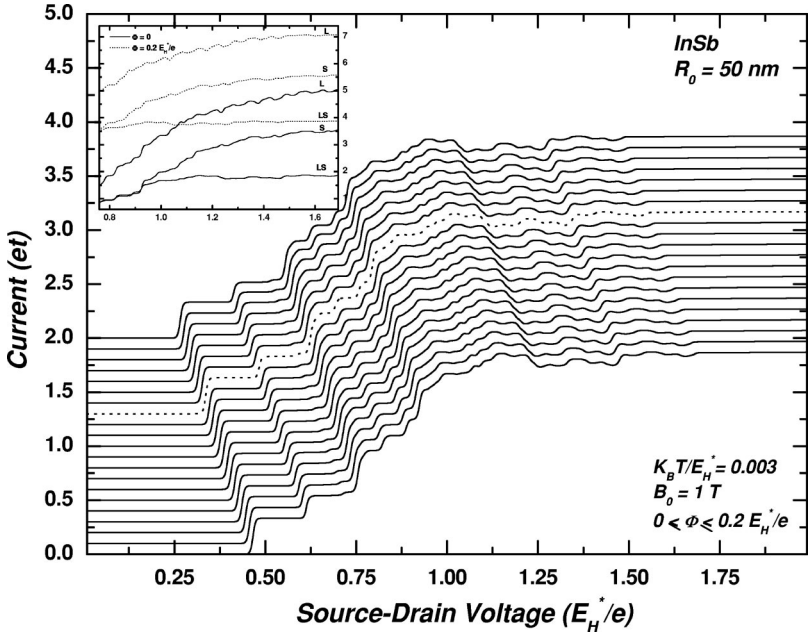


FIG. 6. Influences of a finite gate voltage $\Phi$ in the current curves in the InSb dot with $R_0 = 50$ nm, at finite magnetic field, $B_0 = 1$ T. The plots are shown in steps of 0.01 $E_H^*/e$, ranging from $\Phi = 0$ to 0.2 $E_H^*/e$. The current at $\Phi = 0.13$ $E_H^*/e$, where the suppression of the third plateau has occurred for $B_0 = 0$ case, is shown as a dotted line. The inset compares, at two gate voltages, the influences on the current in different configurations of the Hartree-Fock states in a SQD: $L$ curve (no $S$-selection rules), $S$ curve (no $L$-selection rules), and $LS$ curve (both selection rules).

the voltages where the system reaches full occupation of the ground states for a certain number of carriers in the dot. These magnetic effects are almost negligible for GaAs dots where no significant change can be observed in the transport properties between 0 and 2 T [compare Figs. 1(b) and 5(b)].

The effect of a finite gate voltage in the presence of a magnetic field is shown in Fig. 6. In addition to all general aspects already mentioned in the discussion of Fig. 5, we observe at finite $\Phi$: (i) the transitions which produce the third plateau at zero magnetic field (Fig. 3) are not suppressed in the presence of the field, (ii) the shape of the NDC regions does not change, and (iii) The valleys in the NDC regions at zero $B_0$ are enlarged and the value of the current before and after them is practically the same.

As done for zero magnetic field, the inset of Fig. 6 shows the changes in the overall shapes of the current for the same configurations and voltages discussed in Fig. 3. Here we also see that the $L$ blockade is more effective than the $S$ blockade in the definition of the transport properties of SQD's.

Concerning the influence of the electron-phonon interaction on the overall shape of the $I \times V$ characteristics, we observe that the selection rules [Eq. (26)] involving electron-phonon coupling and the energy conservation will impose stronger restrictions on the allowed transitions. As a consequence of this phonon bottleneck effect, the change on the dot current for any material becomes almost negligible once the probability of a carrier emit or absorb a phonon is rare.[19]

In summary, we have studied the conductance and current curves through a SQD under a magnetic field. The many-particle states and the energy levels are obtained in the strong confined regime by using the $LS$-coupling scheme within the Hartree-Fock approximation. Depending on the absolute value of the $g$ factor of the material, the Zeeman and spin splittings may give origin to level crossings which may alter the energy ordering of the states at high fields. The dependence of $I \times V$ characteristics on temperature and magnetic field in the NDC regions is analyzed as function of the quantum dot parameters and external voltages. The transport properties reflect many characteristics present in the many-particle states, the spatial and spin symmetries, the form of the electron-electron interaction and the magnetic energy as well as the exchange of population between states. We have found that the spherical geometry has lead to an orbital blockade when electron-electron interaction and many-particle eigenstates are considered in the study of the transport properties in SQD's. We may conclude that not only the spin-blockade determines the current but also a crucial role is played by the spatial geometry through the selection rules dictated by the angular momentum conservation of the carriers confined to spherical profiles.

## ACKNOWLEDGMENTS

The authors acknowledge Fundação de Amparo à Pesquisa do Estado de São Paulo (FAPESP) for financial support. C. T-G would like to thanks S. E. Ulloa for helpful and lively discussions.

## APPENDIX

The direct $\Gamma^\kappa$ and exchange $\Lambda^\kappa$ radial integrals of the electron-electron interaction constituting $F^\kappa$ and $G^\kappa$ in Eqs. (20), (21) are defined as

$$\Gamma^\kappa(n_1 l_1, n_2 l_2) = \frac{4}{j^2_{l_1+1}(\alpha_{n_1 l_1}) j^2_{l_2+1}(\alpha_{n_2 l_2})} \int_0^1 \int_0^1 \times dx_1 dx_2 (x_1^2 x_2^2) \left( \frac{x_<^\kappa}{x_>^{\kappa+1}} \right) \times j^2_{l_1}(\alpha_{n_1 l_1} x_1) j^2_{l_2}(\alpha_{n_2 l_2} x_2),$$

$$\Lambda^{\kappa}(n_1 l_1, n_2 l_2) = \frac{4}{j^2_{l_1+1}(\alpha_{n_1 l_1}) j^2_{l_2+1}(\alpha_{n_2 l_2})} \int_0^1 \int_0^1 \times dx_1 dx_2 (x_1^2 x_2^2) \left( \frac{x_<^{\kappa}}{x_>^{\kappa+1}} \right) j_{l_1}(\alpha_{n_1 l_1} x_1) \times j_{l_2}(\alpha_{n_2 l_2} x_1) j_{l_1}(\alpha_{n_1 l_1} x_2) j_{l_2}(\alpha_{n_2 l_2} x_2). \tag{A1}$$

Following Ref. 18, the Coulomb energy contributions for $N=2$ are given by

$$E_C(^1S) = F^0(1s,1s),$$

$$E_C(^3P) = F^0(1s,1p) - \frac{1}{3} G^1(1s,1p),$$

$$E_C(^1P) = F^0(1s,1p) + \frac{1}{3} G^1(1s,1p), \tag{A2}$$

and for $N=3$ they are

$$E_C(^2P) = F^0(1s,1s) + 2F^0(1s,1p) - \frac{1}{3} G^1(1s,1p),$$

$$E_C(^4P) = F^0(1p,1p) + 2F^0(1s,1p) - \frac{1}{5} F^2(1p,1p) - \frac{2}{3} G^1(1s,1p),$$

$$E_C(^2D) = F^0(1p,1p) + 2F^0(1s,1p) + \frac{1}{25} F^2(1p,1p) - \frac{1}{3} G^1(1s,1p),$$

$$E_C(^2S) = F^0(1p,1p) + 2F^0(1s,1p) + \frac{2}{5} F^2(1p,1p) - \frac{1}{3} G^1(1s,1p),$$

$$E_C(^2P') = F^0(1p,1p) + 2F^0(1s,1p) - \frac{1}{5} F^2(1p,1p) + \frac{1}{3} G^1(1s,1p). \tag{A3}$$

As we can see the spatial symmetry and the electron-electron interaction lead to a partial lifting of the degeneracy of the levels $^1P$ and $^3P$ for $N=2$ and $^4P$, $^2D$, $^2S$, and $^2P'$ for $N=3$. The dimensionless values of $\Gamma^{\kappa}$ and $\Lambda^{\kappa}$ for the states in Eqs. (A2) and (A3) are

$$\Gamma^0(1s,1s) = 1.7860731,$$

$$\Gamma^0(1s,1p) = 1.6196770,$$

$$\Gamma^0(1p,1p) = 1.5252119,$$

$$\Gamma^2(1p,1p) = 0.9087439,$$

$$\Lambda^0(1s,1p) = 1.0789639. \tag{A4}$$

Finally, the total energy $E_D$ of a given state will be the sum of the kinetic energy $\varepsilon_{nl} = \hbar^2 \alpha_{nl}^2 / (2m^* R_0^2)$, plus magnetic $E_B$ [see Eq. (22)] and Coulomb $E_C$ contributions. Equations (A2) and (A3) give a straightforward way to know the fractional contribution of the total energy coming from direct and exchange terms in comparison to the confinement and magnetic energies.


[1] D.V. Averin, A.N. Korotkov, and K.K. Likharev, Phys. Rev. B **44**, 6199 (1991).

[2] D. Weinmann, W. Häusler, and B. Kramer, Ann. Phys. (N.Y.) **5**, 652 (1996).

[3] T. Tanamoto and M. Ueda, Phys. Rev. B **57**, 14 638 (1998).

[4] K. Jauregui, W. Häusler, D. Weinmann, and B. Kramer, Phys. Rev. B **53**, R1713 (1996).

[5] W. Häusler and B. Kramer, Phys. Rev. B **47**, 16 353 (1993).

[6] D. Pfannkuche and S.E. Ulloa, Phys. Rev. Lett. **74**, 1194 (1995).

[7] D. Pfannkuche and S. E. Ulloa, *Advances in Solid State Physics* (Vieweg, Braunschweig, 1996), Vol. 35, p. 65.

[8] W. Pfaff, D. Weinmann, W. Häusler, B. Kramer, and U. Weiss, Z. Phys. B: Condens. Matter **96**, 201 (1994).

[9] D. Weinmann, W. Häusler, W. Pfaff, B. Kramer, and U. Weiss, Europhys. Lett. **26**, 467 (1994).

[10] D. Weinmann, W. Häusler, and B. Kramer, Phys. Rev. Lett. **74**, 984 (1995).

[11] C.E. Creffield, W. Häusler, J.H. Jefferson, and S. Sarkar, Phys. Rev. B **59**, 10 719 (1999).

[12] C.E. Creffield, J.H. Jefferson, S. Sarkar, and D.L.J. Tipton, Phys. Rev. B **62**, 7249 (2000).

[13] S. Akbar and In-Ho Lee, Phys. Rev. B **63**, 165301 (2001).

[14] E.B. Foxman, P.L. McEuen, U. Meirav, N.S. Wingreen, Y. Meir, P.A. Belk, N.R. Belk, and M.A. Kastner, Phys. Rev. B **47**, 10 020 (1993).

[15] R.C. Ashoori, H.L. Stormer, J.S. Weiner, L.N. Pfeiffer, K.W. Baldwin, and K.W. West, Phys. Rev. Lett. **71**, 613 (1993).

[16] J.M. Kinaret, Y. Meir, N.S. Wingreen, P.A. Lee, and Xiao-Gang Wen, Phys. Rev. B **46**, 4681 (1992).

[17] C.W.J. Beenakker, Phys. Rev. B **44**, 1646 (1991).

[18] E. U. Condon, and G. H. Shortley, *The Theory of Atomic Spectra* (Cambridge University Press, Cambridge, 1935).

[19] C.F. Destefani and G.E. Marques, Physica E **7**, 786 (2000).